ACS APPLIED MATERIALS & INTERFACES

Research Article

www.acsami.org

Synthesis of Fe_3O_4/Polyacrylonitrile Composite Electrospun Nanofiber Mat for Effective Adsorption of Tetracycline

Qing Liu,[†,‡] Lu-Bin Zhong,[†] Quan-Bao Zhao,[§] Craig Frear,[§] and Yu-Ming Zheng*[,†]

[†]CAS Key Laboratory of Urban Pollutant Conversion, Institute of Urban Environment, Chinese Academy of Sciences, 1799 Jimei Road, Xiamen 361021, China

[‡]College of Resources and Environment, University of Chinese Academy of Sciences, 19A Yuquan RoadBeijing 100049, China

[§]Department of Biological Systems Engineering, Washington State University, Box 646120, Pullman, Washington 99164-6120, United States

Supporting Information

ABSTRACT: Novel Fe_3O_4/polyacrylonitrile (PAN) composite nanofibers (NFs) were prepared by a simple two-step process, an electrospinning and solvothermal method. Characterization by field emission scanning electron microscopy (FESEM) and transmission electron microscopy (TEM) demonstrated formation of a uniform nanoparticles coating (about 20 nm in thickness) on the PAN nanofiber backbone. The coating was constructed by well-crystallized cubic phase Fe_3O_4 nanoparticles as examined by X-ray diffraction spectroscopy (XRD). The coating doubled the specific surface area of NFs, from 8.4 to 17.8 m^2 g^{-1}, as confirmed by nitrogen sorption isotherm analysis. To evaluate the feasibility of Fe_3O_4/PAN composite NFs as a potential adsorbent for antibiotic removal, batch adsorption experiments were conducted using tetracycline (TC) as the model antibiotic molecule. The results showed that Fe_3O_4/PAN composite NFs were effective in removing TC with no impactful loss of Fe in the pH regime of environmental interest (5−8). The adsorption of TC onto Fe_3O_4/PAN composite NFs better fitted the pseudo-second-order kinetics model, and the maximum adsorption capacity calculated from Langmuir isotherm model was 257.07 mg g^{-1} at pH 6. The composite NFs also exhibited good regenerability over repeated adsorption/desorption cycles. Surface complexation between TC and the composite NFs contributed most to the adsorption as elucidated by X-ray photoelectron spectroscopy (XPS). This highly effective and novel adsorbent can be easily modularized and separated, promising its huge potential in drinking and wastewater treatment for antibiotic removal.

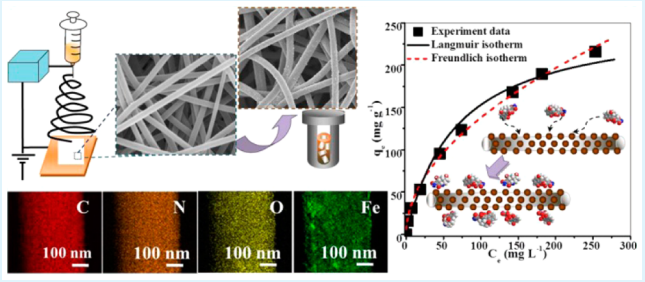

KEYWORDS: *adsorption, antibiotic, electrospinning, nanofiber, solvothermal*

1. INTRODUCTION

Antibiotics are persistent in the natural environment, often in an active state, due to ineffective biological degradation.[1] Their presence within the environment holds potential for inducing antibiotic resistance genes even at trace levels of exposure.[2] To date, many technologies, such as photocatalytic degradation, ion-exchange, membrane filtration, and adsorption, have been explored for the removal of antibiotics from aqueous solution.[3,4] Compared to other techniques, adsorption is considered simple and economical, and remains one of the most attractive methods for antibiotic removal.[4]

Among the currently available adsorbents, iron oxides have been greatly studied due to their outstanding properties like high adsorption capacity, low cost, geological abundance, and environmentally benign nature.[5−7] They are able to form stable metal−ligand complexes with antibiotic molecules, which possess electron-rich functional groups, such as tetracycline (TC).[8] However, separation of iron oxides from an aqueous medium often requires centrifugation which is rather tedious and expensive.[5] Recently, magnetite nanoparticles (MNPs) which can be rapidly separated by magnetic field have been developed for the adsorption of antibiotics and exhibited high adsorption capacities.[9,10] However, for scaled up operation, separation by permanent magnets or magnetized columns still involves high capital investment and/or operational cost, and loss of adsorbents is unavoidable.[11] Therefore, immobilization of active micro- or nanoscale adsorbents appears as a favorable alternative to overcome the difficulty in separation.

One dimensional (1D) electrospun nanofiber (NF) mats produced by high voltage electrospinning technique are macroscale porous materials with numerous fibers in nanoscale range, which can be easily separated from a liquid medium. In addition, due to the extended NF structure, the mats possess a large specific surface area, high porosity, and interconnected

Received: December 19, 2014
Accepted: June 16, 2015
Published: June 16, 2015

DOI: 10.1021/acsami.5b04598
ACS Appl. Mater. Interfaces 2015, 7, 14573−14583

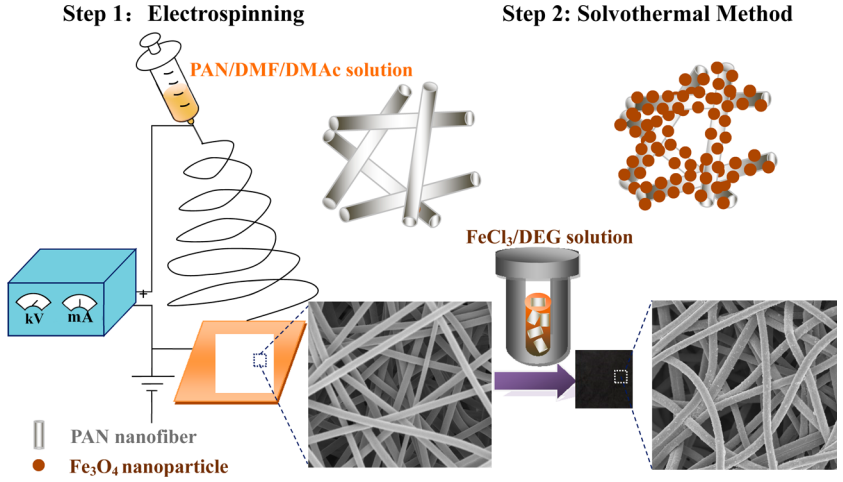

Figure 1. Preparation procedures of Fe_3O_4/PAN composite nanofibers (NFs).

channeling pore structures, which are considered to be excellent supports for nanoparticle (NP) incorporation.[12] The flexibility of NP incorporation by coelectrospinning of a mixture or chemical/physical modification after electrospinning has allowed diversified composition of composite NFs and their various applications in energy production,[13] fluid separation,[14] catalysis,[15] gas sensors,[16] and supercapacitors.[17] Lately, increasing interest has been drawn to the application of composite NFs for water treatment, in particular, removal of organic pollutants.[18,19] For example, Chen et al. have reported the effective adsorption of Congo red by calixarene-functionalized polyacrylonitrile (PAN) NFs.[18] However, to our best knowledge, removal of antibiotics by electrospun NFs has not been thoroughly studied yet.

In the present study, we report novel composite 1D nanostructured Fe_3O_4/PAN composite NFs combining the merits of Fe_3O_4 NPs and electrospun PAN NFs, which have high adsorption capacity and are easy for separation from aqueous media, respectively. PAN is chosen as the template for Fe_3O_4 NP deposition due to its low cost, ease of electrospinning, and high tensile strength after electrospinning,[20] making it suitable for water treatment. Figure 1 illustrates the design and fabrication procedure of Fe_3O_4/PAN composite NFs. First, PAN NFs were prepared via electrospinning technique. Next, uniform layers of Fe_3O_4 NPs were formed and simultaneously deposited on PAN NF surface via solvothermal treatment. The adsorption performance of the as-synthesized Fe_3O_4/PAN composite NFs was examined via removal of TC, a widely used broad-spectrum antibiotic and an important contaminant in aquatic systems.[21] The maximum adsorption capacity was calculated to evaluate the feasibility of Fe_3O_4/PAN composite NFs as a promising antibiotic adsorbent. The underlying adsorption mechanism was explored by examining the adsorption behavior under varying solution pH and with the aid of X-ray photoelectron spectroscopy (XPS).

2. EXPERIMENTAL SECTION

2.1. Chemical Reagents. Anhydrous ferric chloride ($FeCl_3$), trisodium citrate ($Na_3C_6H_5O_7$, Na_3Cit), anhydrous sodium acetate (CH_3COONa), ethanol (C_2H_6O), diethylene glycol (DEG), sodium chloride (NaCl), sodium hydroxide (NaOH), hydrochloric acid (HCl), *N*,*N*-dimethylformamide (DMF), and *N*,*N*-dimethylacetamide (DMAc) were of analytical grade and purchased from Sinopharm Chemical Reagent Co. Ltd. (Shanghai, China). Polyacrylonitrile (PAN, M_w = 90 000) was commercially available from Kunshan Hong Yu Plastic Co. Ltd. (Suzhou, China). Tetracycline hydrochloride ($C_{22}H_{24}N_2O_8$·HCl, USP grade) was obtained from Amresco (Ohio). Milli-Q element ultrapure water (18.2 Ω, Millipore, Massachusetts) was used to prepare all solutions. All materials were used as-received without further treatment.

2.2. PAN NFs Fabrication. PAN solution (10 wt %) was prepared by dissolving PAN powder in the mixed solvent of DMF and DMAc (w:w ratio,1:1). The resultant solution was continuously stirred in a Yuhua thermostat water bath (Henan, China) at 60 °C for 2 h. The PAN/DMF/DMAc solution was transferred to a 10 mL syringe connected with a 19-gauge metal needle. The feeding rate was controlled at 0.9 mL/h by a Veryark TCI-IV syringe pump (Guangxi, China). A high voltage supply of 12 kV was constantly applied between the needle tip and a grounded rotating metal drum wrapped with aluminum foil. The distance between the needle tip and the collecting drum was 15 cm. The fibrous mat was collected after 8 h electrospinning to ensure similar thickness of PAN NFs.

2.3. Preparation of Fe_3O_4 NPs and Fe_3O_4/PAN Composite NFs. Fe_3O_4 NPs were synthesized by a modified literature method.[22] In brief, 1.300 g of anhydrous $FeCl_3$ was first dissolved in 80 mL of DEG under vigorous stirring at 80 °C until a homogeneous solution was formed. Next, 1.162 g of Na_3Cit was added; when a clear solution was obtained, 1.969 g of anhydrous sodium acetate was introduced subsequently to the mixture. Temperature was maintained at 80 °C throughout the process. The obtained solution was then transferred to a Teflon-lined stainless steel autoclave with a volume of 100 mL. PAN NFs (0.1 g) were cut to 5 cm × 2 cm, and immersed in the solution. The autoclave was sealed and heated at 200 °C for 14 h. After natural cooling of the autoclave, both Fe_3O_4 NPs and Fe_3O_4/PAN composite NFs were obtained. The black Fe_3O_4 NPs were collected by a permanent magnet and washed with ethanol four times, and the final products were obtained after 24 h of freeze-drying. Fe_3O_4/PAN composite NFs were retrieved by a tweezer and washed with deionized water several times. After drying at 60 °C for 24 h, Fe_3O_4/PAN composite NFs were ready for further experiment. $FeCl_3$ to PAN NF dosage ratio was optimized in the preliminary experiments (Table S1 and Figures S1 and S2, Supporting Information).

2.4. Characterization. The morphologies and element composition of PAN NFs and Fe_3O_4/PAN composite NFs were acquired by a Hitachi S-4800 field emission scanning electron microscopy (FESEM) with an energy dispersive X-ray spectrometer (EDAX) (Genesis, XM2). The surface of the samples was coated with platinum for 30 s by an EMS 150T ES turbo pumped sputter coater (Pennsylvania). Transmittance electron microscope (TEM) photographs of the samples were examined by a Philips Tecnai F20 (Oregon) or Carlzeiss EM912ΩEF-TEM (Germany). X-ray diffraction (XRD) patterns were collected using a PANalytical X' Pert PRO (Almelo, The Netherlands)

DOI: 10.1021/acsami.5b04598
ACS Appl. Mater. Interfaces 2015, 7, 14573−14583

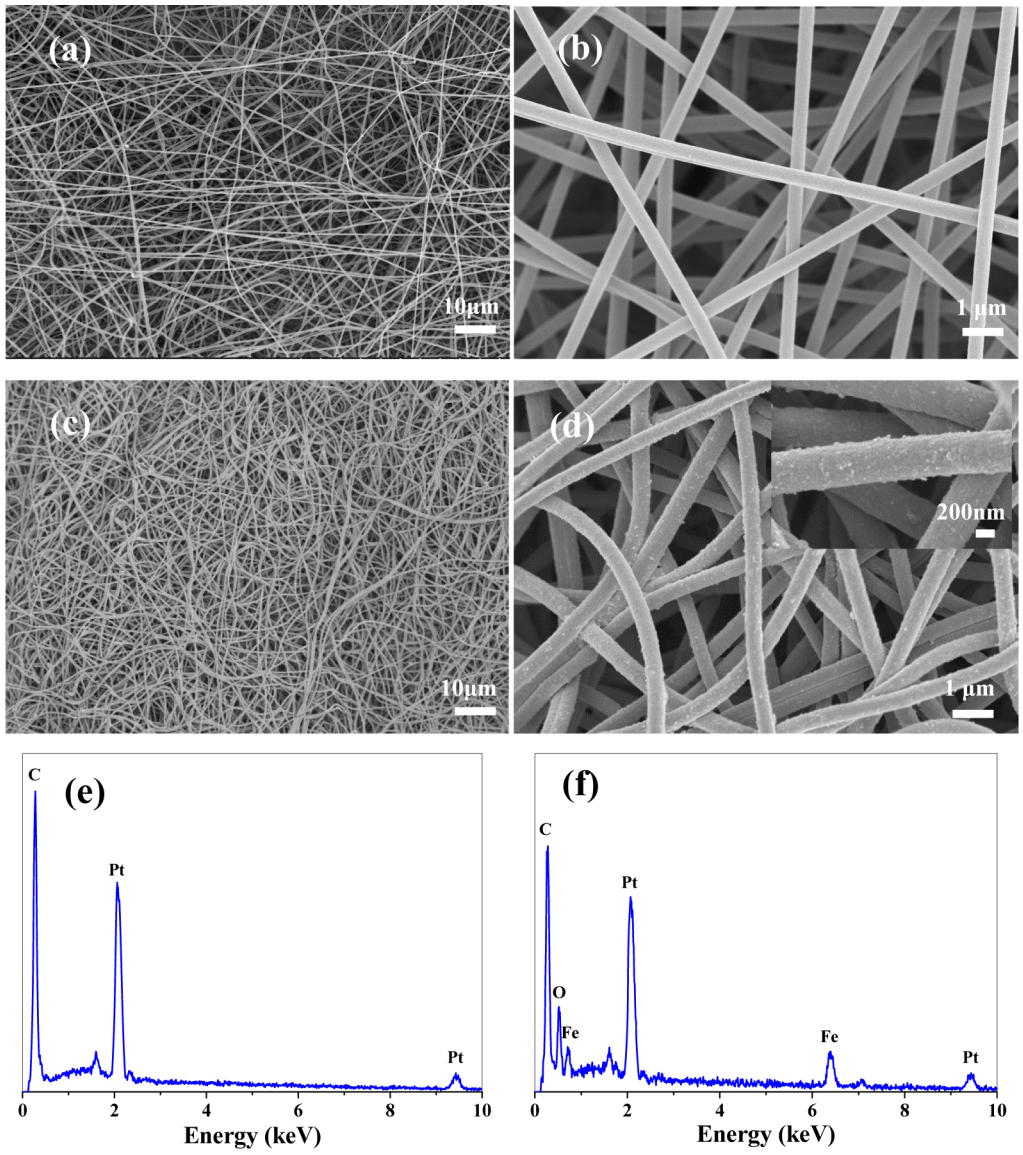

Figure 2. Morphology and element composition of electrospun NFs: (a) the panoramic FESEM and (b) magnified (10.0k×) images of PAN NFs; (c) the panoramic FESEM and (d) magnified (10.0k×) images of Fe_3O_4/PAN composite NFs, and magnified (50.0k ×) image of Fe_3O_4 NPs (d inset); EDAX element composition analysis of (e) PAN NFs and (f) Fe_3O_4/PAN composite NFs.

X-ray diffractometer with a Ni filter, Cu Kα radiation source (λ = 0.154 060 nm), and angular variation of 10−80° operated at a tube voltage of 40 kV and a tube current of 40 mA. Nitrogen adsorption−desorption isotherms were conducted at 77 K with a Micromeritics ASAP2020 M+C surface area and porosity analyzer (Georgia). The specific surface areas of PAN and Fe_3O_4/PAN composite NFs were calculated according to the Brunauer−Emmett−Teller (BET) method. The pore size distribution was derived from the desorption branch of the isotherm with the Barrett−Joyner−Halenda (BJH) model. The thermal stability and relative Fe content of the composite NFs were investigated by thermogravimetric analysis (TGA) with a Netzsch Tartus TG209 F3 Analyzer (Germany). TGA was conducted from 40 to 900 °C with a heating rate of 10 °C min^{-1} and a constant air flow of 60 mL min^{-1}. XPS spectra were collected using a PHI Quantum-2000 electron spectrometer (Ulvac-Phi, Japan) with 150 W monochromatized Al Kα radiation (1486.6 eV).

2.5. TC Adsorption on Fe_3O_4/PAN Composite NFs. To evaluate the efficiency of Fe_3O_4/PAN composite NFs for TC adsorption in aqueous solution, a series of batch adsorption experiments responded to the impacts of several parameters; that is, contact time, solution pH, and initial TC concentration experiments were conducted. Generally, a series of 10 mg of Fe_3O_4/PAN composite NFs were added to 100 mL glass bottles containing 20 mL of TC solutions. The glass bottles were wrapped with aluminum foil to avoid light exposure and shaken at 150 rpm and 25 °C until the equilibrium was established. The equilibrium solutions were filtered through 0.45 μm membrane filters and analyzed for the residual TC concentration. TC concentrations before and after adsorption were determined by a Puxi TU-1810 UV−vis spectrometer (Beijing) at 358 nm. Our preliminary study (adsorbent free) revealed that the loss of TC due to glass adsorption and filter interception was less than 5% under the applied experiment condition (data not shown).

In the pH effect study, solution pH was adjusted to and maintained at 3−11 by 0.1 M HCl or 0.1 M NaOH solution. The initial concentration of TC was kept at 22 mg L^{-1}. The experiments were conducted in duplicate to ensure the reliability of the results. To investigate the adsorption capacity of adsorbent, Fe_3O_4/PAN composite NFs were added to a number of TC solutions with initial concentration varying from 10 to 360 mg L^{-1}. Solution pH was initially adjusted to 6.00 ± 0.05 and maintained during the isotherm experiment. The equilibrium adsorption amounts of TC were calculated by eq 1

DOI: 10.1021/acsami.5b04598
ACS Appl. Mater. Interfaces 2015, 7, 14573−14583

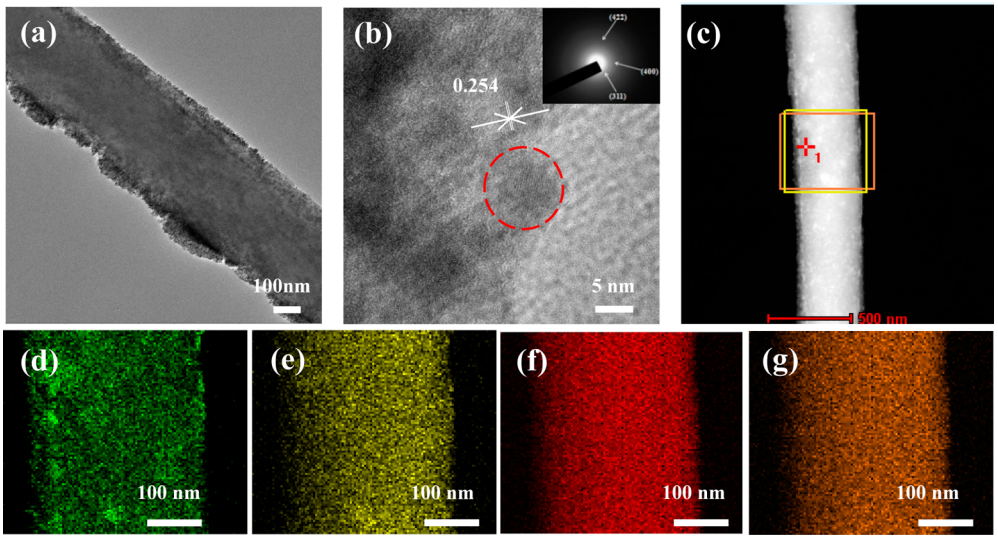

Figure 3. TEM images of (a) the Fe_3O_4/PAN composite NFs; (b) typical HR-TEM image and the SAED of Fe_3O_4 NPs on the Fe_3O_4/PAN composite NFs surface (top right corner inset); (c) SSEM image of the Fe_3O_4/PAN composite NFs; (d–g) EDX elemental mappings of Fe, O, C, and N, respectively. The red circle represents one Fe_3O_4 nanoparticle.

$$q_e = \frac{(C_0 - C_e)V}{m} \quad (1)$$

where q_e (mg g^{-1}) is the amount of TC adsorbed at equilibrium, C_0 and C_e (mg L^{-1}) are the concentration of TC at initial and equilibrium, respectively, V is the volume of TC solution, and m is the weight of Fe_3O_4/PAN composite NFs. Residual Fe in TC solution was determined by a PerkinElmer Optima 7000 DV ICP-OES (Massachusetts).

The adsorption kinetics experiment was carried out with the same operating conditions as the equilibrium studies. A 100 mg portion of Fe_3O_4/PAN composite NFs was added to 200 mL of TC solution with initial concentration of 22 mg L^{-1} and initial pH of 6.01. There were 1.5 mL aliquots drawn at predetermined time intervals and filtered through 0.45 μm membrane filters. TC concentrations of all samples were measured, and the amounts of TC adsorbed at specific time were determined by eq 2

$$q_t = \frac{(C_0 - C_t)V}{m} \quad (2)$$

where q_t (mg g^{-1}) is the amount of TC adsorbed at time t, and C_t (mg L^{-1}) is the concentration of TC at time t.

The point of zero charge pH (pH_{pzc}) of Fe_3O_4/PAN composite NFs was determined by the immersion technique.[23] Briefly, a number of aqueous solutions (20 mL) were prepared with a background electrolyte (NaCl) concentration of 0.05 M. The electrolyte solutions were then adjusted to an initial pH value of 4, 5, 6, 7, 8, 9, or 10 using 0.1 M NaOH or 0.1 M HCl solution where appropriate. A 10 mg portion of Fe_3O_4/PAN composite NFs was added to each solution, and the solutions were equilibrated at 25 °C until an equilibrium pH was reached. The change in pH during equilibration, ΔpH (difference between the final and initial pH) was then plotted against the initial pH. The initial pH at which ΔpH equaled to zero was taken as the pH_{pzc}. The experiment was conducted in duplicate to ensure the reliability of the results.

For regeneration, Fe_3O_4/PAN composite NFs were retrieved by a tweezer from TC solution and washed with distilled water. NaOH solution (0.01 M, 25 mL), chosen as the desorption agent, was mixed with Fe_3O_4/PAN composite NFs and shaken at 140 rpm for 0.5 h. The membranes were then retrieved and washed with distilled water until a neutral state was obtained. The experiment was conducted in duplicate to ensure the reliability of the results.

3. RESULTS AND DISCUSSION

3.1. Morphology and Composition Analysis. Figure 2a illustrates the morphological characteristic of electrospun PAN

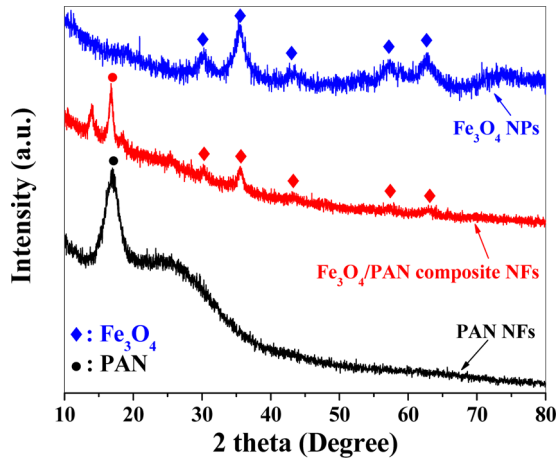

Figure 4. XRD patterns of PAN NFs, Fe_3O_4 NPs, and Fe_3O_4/PAN composite NFs.

NFs, which are long, continuously cylindrically shaped, and randomly distributed. The mat was beadless with an average NFs diameter of 464.1 ± 40.8 nm. The enlarged image (Figure 2b) shows that the NFs are well-aligned with a relatively smooth surface. After solvothermal treatment, the average fiber diameters are 458.0 ± 38.2 nm (Figure 2c), which is very close to PAN NFs; however, the straight and smooth PAN NFs turned wavier and rougher due to the formation of Fe_3O_4 NPs on the PAN NFs surface (Figure 2d). The inset in Figure 2d shows that the Fe_3O_4 NPs are spherical in shape with relatively uniform size of 40–50 nm, which can significantly increase the specific surface area of PAN NFs. EDAX analysis (Figure 2e,f) confirms the formation of iron oxide on PAN NFs after the solvothermal treatment.

TEM micrographs further reveal the presence of uniform Fe_3O_4 NP layers on the surface of the PAN NF backbone (Figure 3a). The diameter of a single NF is around 500 nm,

DOI: 10.1021/acsami.5b04598
ACS Appl. Mater. Interfaces 2015, 7, 14573–14583

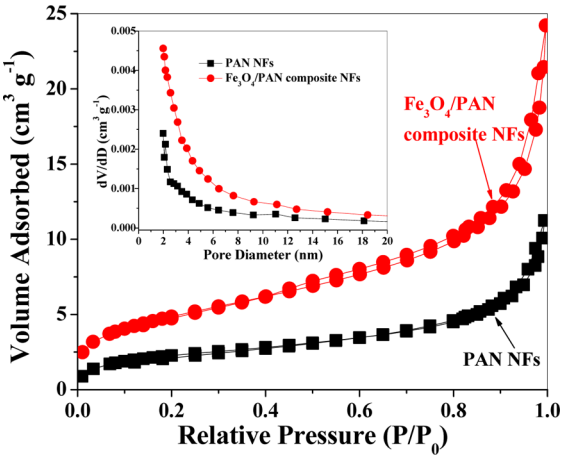

Figure 5. Nitrogen adsorption and desorption isotherms of PAN NFs and Fe_3O_4/PAN composite NFs with the corresponding pore-size distributions (inset) calculated by BJH method.

which is consistent with the SEM observation. The thickness of the coating is about 20 nm while the size of the Fe_3O_4 NPs is estimated to be around 60 nm. Figure 3b shows a typical high resolution TEM (HR-TEM) image of the surface edge of Fe_3O_4/PAN composite NFs, confirming the surface layer of NFs is composed of Fe_3O_4 NPs with an average size about 10 nm as indicted in the red circle. This coating of the Fe_3O_4 NP layer provides numerous active sites on the PAN NF backbone, allowing for the interaction with TC. Meanwhile, Fe_3O_4 NPs enhanced surface roughness, consequently increasing the surface area of composite NFs, which in turn could also enhance the capability of pollutant removal. HR-TEM analysis dictates that the nanoparticle is a highly ordered single-domain crystal. The interplanar distance between two adjacent lattice fringes is measured as 0.254 nm, corresponding well to the lattice spacing of (311) planes of a face-centered cubic (fcc) of Fe_3O_4.[22] Selected-area electron diffraction (SAED) pattern dictates that the polycrystalline diffraction rings are relative to the indices of the lattice planes of the fcc phase (Figure 3b, inset). EDX elemental mappings (Figure 3c–g) confirm that the heterogeneous structures of composite NFs are formed by the PAN NF backbone which consists of C and N elements, and a uniformed surface coating of Fe_3O_4 NPs which is composed of two elements: Fe and O.

XRD was performed in addition to investigating the phase structures of the as-synthesized Fe_3O_4/PAN composite NFs. Figure 4 shows that both bare PAN NFs and Fe_3O_4/PAN composite NFs possess the same diffraction peak at $2\theta = 16.7°$, corresponding to the (200) plane of PAN.[20,24] The as-synthesized Fe_3O_4/PAN composite NFs show the diffraction peaks of the fcc phase of Fe_3O_4 (JCPDS no. 082-1533), i.e., 30.2° (220), 35.6° (311), 43.4° (400), 57.2° (511), 63.0° (440).[17,25] The diffraction peaks also match well with synthesized Fe_3O_4 NPs. According to the Debye–Scherrer formula, the average size of crystallites is estimated on the basis of broadening of the corresponding X-ray diffraction peaks by eq 3

$$D = \frac{K\lambda}{\beta \cos\theta} \tag{3}$$

where D is the grain size (nm), λ is the wavelength of the X-ray radiation (Cu Kα = 0.154 060 nm), K is the Scherrer constant ($K = 0.9$), θ is the X-ray diffraction angle, and β is the full-width at half-maximum (fwhm) of the (311) plane. The crystal size is estimated to be 9.1 nm, which is in good agreement with the HRTEM and SAED observations discussed earlier.

Nitrogen adsorption–desorption measurements were carried out to determine the specific surface areas and pore sizes of PAN NFs and Fe_3O_4/PAN composite NFs (Figure 5). The obtained isotherm of PAN NFs exhibited type II (IUPAC nomenclature) structure, indicating that the electrospun NFs are macroporous with no internal micropores. Instead, Fe_3O_4/PAN composite NFs displayed a type IV hysteresis loop at a relative pressure range 0.45–0.95, which confirmed the existence of mesopores.[26] With the coating of the Fe_3O_4 NP layer, the BET surface area of Fe_3O_4/PAN composite NFs is doubled compared to that of PAN NFs, increasing from 8.4 to 17.8 m^2 g^{-1}. The corresponding pore size distributions calculated from the desorption branch of nitrogen isotherms by the BJH method are presented in the inset of Figure 5. The average pore sizes of PAN and Fe_3O_4/PAN composite NFs are 8.65 and 8.67 nm, respectively.

3.2. TC Adsorption Performance Studies. *3.2.1. Effect of pH.* Preliminary study has revealed that bare PAN NFs were not effective to remove TC as shown in Figure S3 (Supporting Information). The adsorption capacity of TC on PAN NFs is 2.30 ± 0.25 mg g^{-1}, which is much lower than that on the Fe_3O_4/PAN composite NFs (38.54 ± 0.57 mg g^{-1}) under the

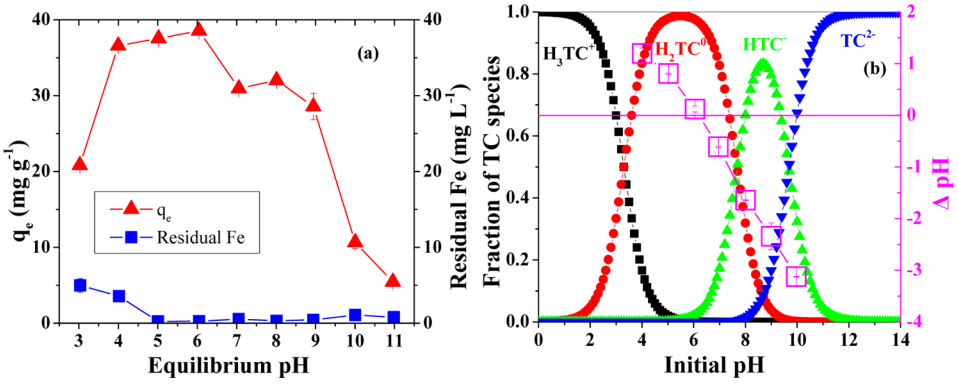

Figure 6. (a) Tetracycline (TC) adsorption capacities of Fe_3O_4/PAN composite NFs and residual Fe in solution with varying pH. Experimental conditions: adsorbent dose = 0.5 g L^{-1}; initial TC concentration = 22 mg L^{-1}. (b) Chemical species distribution of TC at different pH and determination of pH$_{pzc}$ on the basis of immersion technique. Experimental conditions: adsorbent dose = 0.5 g L^{-1}; NaCl concentration = 0.05 M. Error bars stand for standard deviations of duplicate samples.

DOI: 10.1021/acsami.5b04598
ACS Appl. Mater. Interfaces 2015, 7, 14573–14583

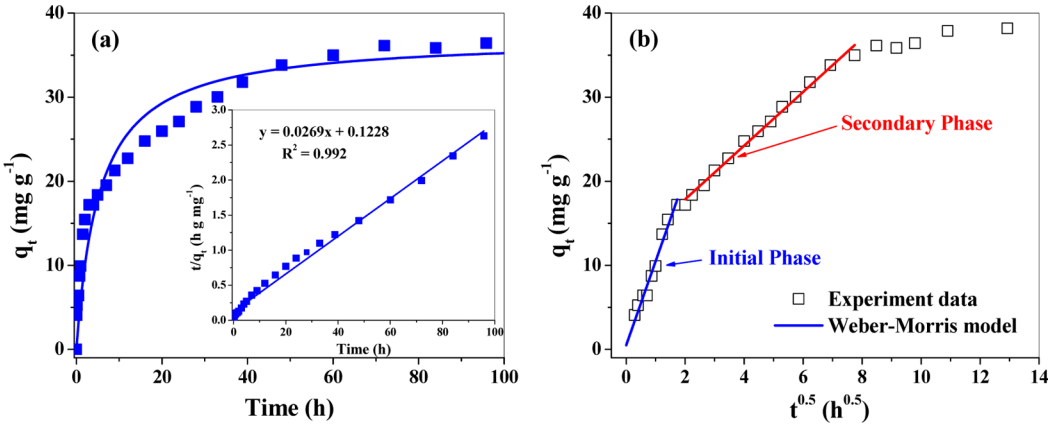

Figure 7. (a) Adsorption kinetics of TC on Fe_3O_4/PAN composite NFs. Experimental conditions: adsorbent dose = 0.5 g L^{-1}; initial TC concentration = 22 mg L^{-1}; initial pH = 6.01. The solid line is pseudo-second-order fit to the experiment data. The inset stands for the linear fit of the model. (b) Weber–Morris kinetics modeling of TC adsorption.

Table 1. Parameters of Kinetic Models

	pseudo-first-order kinetics model			pseudo-second-order kinetics model		
$q_{e,exp}$ (mg g^{-1})	$q_{e,c}$ (mg g^{-1})	$k_1 \times 10^{-2}$ (h^{-1})	R^2	$q_{e,c}$ (mg g^{-1})	$k_2 \times 10^{-4}$ (g mg^{-1} h^{-1})	R^2
36.43	27.77	5.11	0.9627	37.17	58.9	0.9916
	Initial Phase			Secondary Phase		
Weber–Morris model	K_{d1} (mg g^{-1} $h^{-1/2}$)	I_1	R^2	K_{d2} (mg g^{-1} $h^{-1/2}$)	I_2	R^2
	9.77	0.761	0.9627	3.34	10.938	0.9975

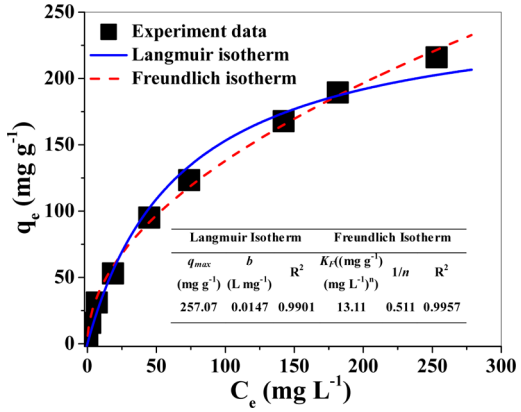

Figure 8. Adsorption isotherm of TC on Fe_3O_4/PAN composite NFs. Experimental conditions: adsorbent dose = 0.5 g L^{-1}; initial TC concentration = 22 mg L^{-1}; initial pH = 6.00 ± 0.05.

Table 2. Maximum Tetracycline Adsorption Capacities of Previously Reported Adsorbents

adsorbent	$C_{0,max}$ (mg TC L^{-1})	pH	T (°C)	q_{max} (mg g^{-1})	ref
dual-functional chelating resin	266.7[a]	5.0	25	4.89[a]	29
nitrifying granules	50	n.m.[b]	25	9.51	39
bamboo charcoal	100	7.0	30	22.7	40
chitosan powder	471.1[a]	6.7	25	23.92[a]	41
mesoporous BiOI microsphere	80[c]	n.m.	25	28.35	3
Fe_3O_4-rGO	75	n.m.	25	95	42
graphene oxide	333.3	3.6	25	313.48	30
Fe_3O_4/PAN composite NFs	360	6.0	25	257.07	this work
Fe_3O_4 magnetite nanoparticles	n.m.	6.5	25	500	10

[a]Converted from mmol. [b]Not mentioned. [c]Calculated on the basis of the isotherm plot.

same experimental condition. In the composite Fe_3O_4/PAN NFs, Fe_3O_4 NPs can effectively adsorb TC through formation of stable metal–ligand complex,[8] while PAN NFs provides the support for NP deposition. In a comparison with free Fe_3O_4 NPs which tend to aggregate and cannot be fully recovered from an aqueous medium, the composite NFs can be easily separated, and the recovery of NPs is high.[10]

TC adsorption on metal oxide was reported to be highly influenced by solution pH.[5−7] The change of pH can affect the speciation of TC and the surface properties of Fe_3O_4/PAN composite NFs, for example, the amount of hydroxyl moieties on its surfaces.[27] In this study, similar pH-dependent behavior of TC adsorption on Fe_3O_4/PAN composite NFs was also observed (Figure 6a). By evaluating the change in surface charges, the observed pH dependence could be rationalized.

According to the point of zero charge pH (pH_{pzc}) characterization (Figure 6b), the pH_{pzc} value of Fe_3O_4/PAN composite NFs was determined as 6.1, implying that the adsorbent was positively charged when solution pH was below 6.1, and was negatively charged as pH was above 6.1. When the solution pH is below the pK_{a1} (3.30) value of TC (Scheme S1, Supporting Information), the dominant species of TC in water is TCH_3^+ (Figure 6b), while the hydroxyl moieties on the surfaces of Fe_3O_4/PAN composite NFs mainly exist in the positively charged form ($-OH_2^+$). The dominant electrostatic interaction between TC and Fe_3O_4/PAN composite NFs should be repulsion at low pH. However, there is still a considerable amount of TC (20.83 ± 0.36 mg g^{-1}) adsorbed on Fe_3O_4/PAN composite NFs surfaces at pH 3, indicating that, besides the electrostatic interaction, some cation exchange

DOI: 10.1021/acsami.5b04598
ACS Appl. Mater. Interfaces 2015, 7, 14573−14583

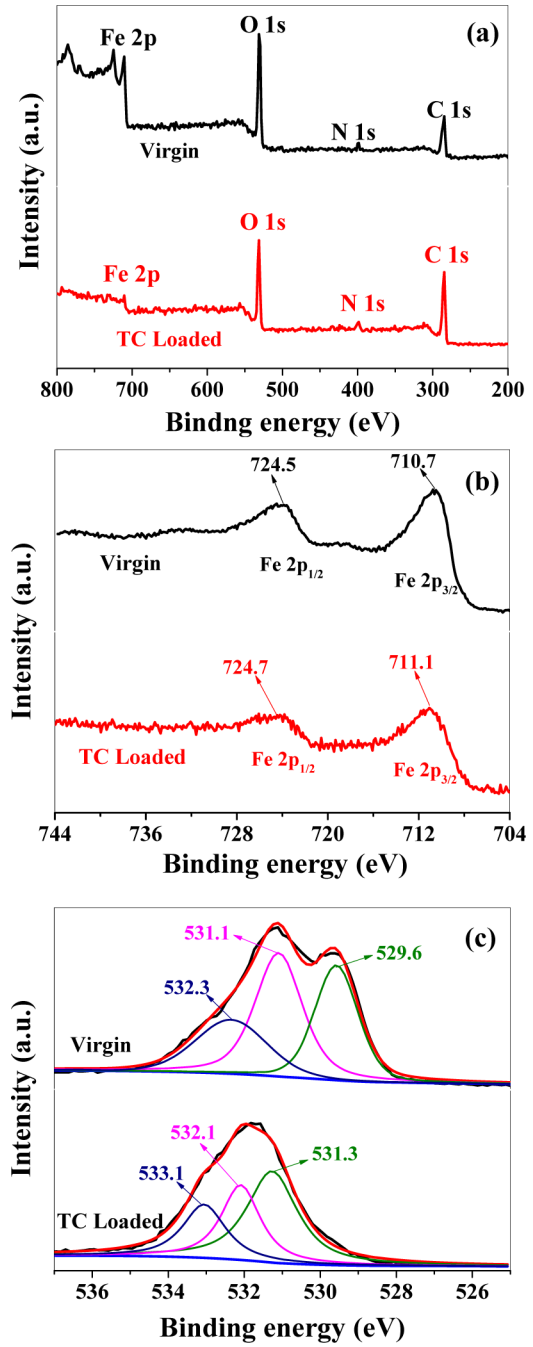

Figure 9. (a) XPS wide-scan spectra, high resolution (b) Fe 2p, and (c) O 1s XPS spectra of Fe_3O_4/PAN composite NFs.

Table 3. Binding Energy and Relative Content of O in Fe_3O_4/PAN Composite Nanofibers

valence state	sample	proposed components	binding energy (eV)	relative content (%)
O 1s	virgin NFs	Fe−O	529.6	33.2
		H−O	531.1	42.6
		C−O	532.3	24.2
	TC-loaded NFs	Fe−O	531.3	46.9
		H−O	532.1	29.9
		C−O	533.1	23.2

could occur between the C4 dimethylammonium group of TC and the hydroxyl moiety ($-OH_2^+$) of Fe_3O_4/PAN composite NFs surfaces.[28] As shown in Figure 6a, the residual Fe ion concentration in the aqueous solution is rather high at low pH ($\leq$4). It is likely caused by the loss of Fe_3O_4 NPs at strong acidic conditions, which could, in addition, contribute to the low adsorption capacity observed. When solution pH increases from 3.30, the adsorption capacity increases tremendously with the highest adsorption capacity (38.53 ± 0.57 mg g^{-1}) found at pH 6. At pH around 6, the dominant TC species is TCH_2, and the composite NF surface is neutrally charged. Hence, the lowest electrostatic repulsion is experienced at pH around 6, resulting in the highest adsorption capacity, which is consistent with the observation on Fe_3O_4 MNPs.[10] Furthermore, TC complexation with iron oxide has also been reported to occur at many binding sites, such as the deprotonated C1−C3 tricarbonyl methane moiety and the C10−C12 phenolic diketone moiety.[6] Hence, the highest adsorption capacity of TC on Fe_3O_4/PAN composite NFs is obtained. When pH further increases from 6, the dominant species become TCH^- and TC^{2-}, and the surface of composite NFs also becomes negatively charged. The increase in the proportion of negatively charged TC species and negative charges on the surfaces of Fe_3O_4/PAN composite NFs results in a stronger electrostatic repulsion; thus, there is a reduced adsorption affinity of TC to Fe_3O_4/PAN composite NFs. However, some specific interaction, such as surface complexation, can still be formed, probably between Fe ions and the C10−C12 phenolic diketone moiety.[28]

To evaluate the stability of adsorbent and examine a possible secondary pollution, the residual Fe concentration in TC solution was measured. It is observed that, at strong acidic condition, H^+ is able to react with Fe_3O_4 and cause leaching of Fe ions into the solution (Figure 6a). Hence, the composite NFs are not suitable for application under low pH. However, when pH increases to 5 and above, leaching of Fe ion significantly reduces. The composite NFs are stable when the pH is above 5, and residual Fe concentration is not of health concern at this level according to WHO Guidelines for Drinking Water Quality. Considering the pH regime of environmental interest, such as groundwater (pH 5.5) to typical wastewater treatment plant operating condition (pH 6.5−8),[4] we conclude that Fe_3O_4/PAN composite NFs can be used for TC adsorption in various aqueous systems. With the above considerations and goal of a more practical study, equilibrium pH at 6 was fixed in the subsequent kinetics and equilibrium isotherm studies.

3.2.2. Adsorption Kinetics. The adsorption kinetics of TC on Fe_3O_4/PAN composite NFs was illustrated in Figure 7a. TC adsorption rapidly increased during the first 5 h, and over 50% of the equilibrium adsorption capacity was achieved. Subsequently the adsorption rate declined, and the equilibrium was reached within 72 h. Two commonly used kinetics models, pseudo-first-order and pseudo-second-order kinetics models, were applied to interpret kinetics data.[29] Their expressions are given by eqs 4 and 5, respectively.

$$q_t = q_e - q_e e^{-k_1 t} \quad (4)$$

$$q_t = \frac{k_2 q_e^2 t}{1 + k_2 q t} \quad (5)$$

DOI: 10.1021/acsami.5b04598
ACS Appl. Mater. Interfaces 2015, 7, 14573−14583

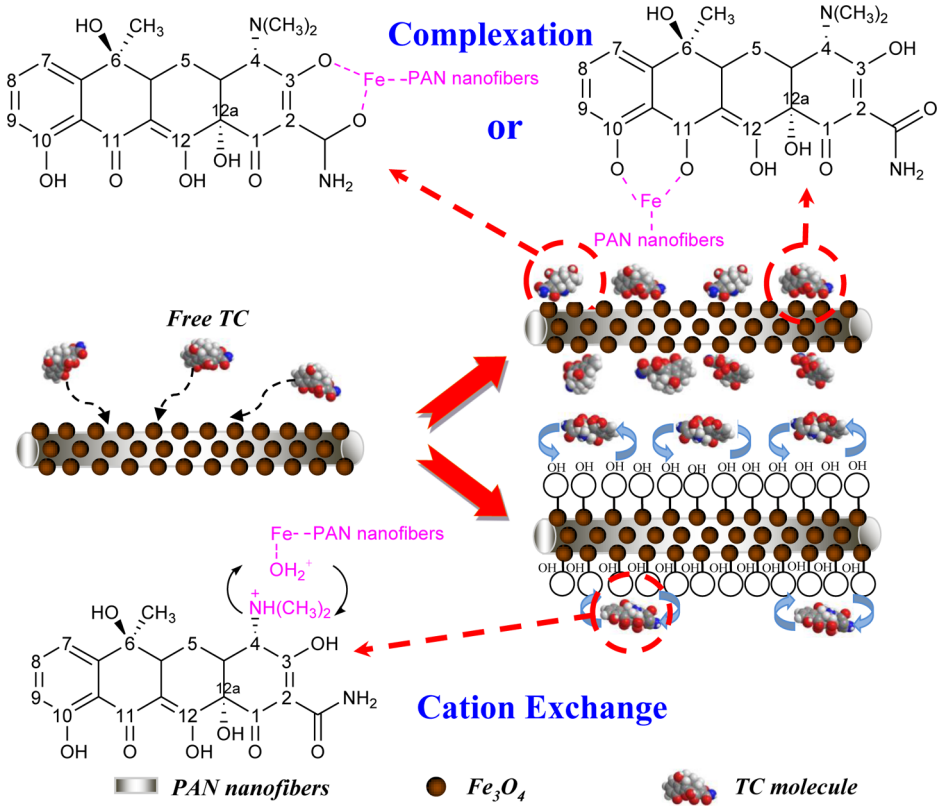

Figure 10. Mechanistic illustration of adsorption of TC on Fe_3O_4/PAN composite NFs.

Here k_1 and k_2 (g mg^{-1} h^{-1}) are the equilibrium rate constant associated with pseudo-first-order and pseudo-second-order sorption, respectively, q_e and q_t are the amount of TC adsorbed at equilibrium and time t, respectively, and $k_2q_e^2$ is the initial rate (mg g^{-1} h^{-1}) in the pseudo-second-order model. The linear forms of eqs 4 and 5 are presented by eqs 6 and 7 below.

$$\ln(q_e - q_t) = \ln q_e - k_1 t \tag{6}$$

$$\frac{t}{q_t} = \frac{1}{k_2 q_e^2} + \frac{t}{q_e} \tag{7}$$

The values of k_1, k_2, and q_e can be calculated from eqs 6 and 7, and are presented with the linear regression values in Table 1. As shown in Table 1 and the inset of Figure 7a, the adsorption kinetics data can be better fitted to the pseudo-second-order model ($R^2 > 0.99$), indicating that the rate-limiting step in the TC adsorption process may be chemisorption.[30] It is proposed that surface complexation with specific sorption sites, in this case, Fe_3O_4 NP layers on NF surface, was involved during the adsorption process.[31]

In addition, the Weber–Morris model is employed to further analyze the adsorption kinetics and to assess the importance of diffusion during the adsorption process (Figure 7b). The Weber–Morris model equation is presented in eq 8.[32]

$$q_t = K_d t^{0.5} + L \tag{8}$$

Here, K_d and L represent the intraparticle diffusion coefficient and the thickness of boundary layer, respectively. Hence, a larger L indicates a stronger effect by boundary layer. Prior to equilibrium, a plot of q_t versus $t^{0.5}$ in Figure 7b displays multiple linearities; thus, the adsorption process can be divided into two different phases. The Weber–Morris model is applied to both phases, and the kinetic constants are summarized in Table 1. Both phases fit well to the Weber–Morris model ($R^2 > 0.97$). The initial phase is attributed to the diffusion of TC through the solution to the exterior surface of the composite NFs, which can be regarded as external diffusion. The secondary stage shows the gradual adsorption where intraparticle diffusion is rate-limiting.[32] Clearly, intraparticle diffusion was the dominant rate-limiting process in TC adsorption on the Fe_3O_4/PAN composite NFs.

3.2.3. Adsorption Isotherm. The adsorption isotherm experiment at different TC concentrations (10–360 mg L^{-1}) was conducted to determine the maximum adsorption capacity of Fe_3O_4/PAN composite NFs. Both Langmuir and Freundlich isotherm models are applied to analyze the adsorption process of TC to the composite NFs, which are presented in eqs 9 and 10, respectively.[29,33]

$$q_e = \frac{bq_{max}C_e}{1 + bC_e} \tag{9}$$

$$q_e = K_f C_e^{1/n} \tag{10}$$

Here q_e (mg g^{-1}) is the TC adsorption amount at equilibrium, q_{max} (mg g^{-1}) is the capacity representing a full monolayer coverage of adsorbent surface according to Langmuir isotherm, C_e is the concentration of TC at equilibrium, b is a measure of the energy of adsorption, K_f is adsorption constant of Freundlich isotherm, and n is the Freundlich linearity index.

The experimental isotherm data and Langmuir and Freundlich model fits with the isotherm constants and correlation coefficients are presented in Figure 8. The model is better fitted to the Freundlich model, suggesting a possible multilayer adsorption of TC molecules on the surfaces of

DOI: 10.1021/acsami.5b04598
ACS Appl. Mater. Interfaces 2015, 7, 14573–14583

Fe_3O_4/PAN composite NFs. With the assumption that a TC molecule occupies a projected surface area of 190 Å^2,[5] on the basis of the molecular weight of TC and BET surface area obtained earlier, the monolayer coverage of TC on Fe_3O_4 NFs surface is estimated to be 6.92 mg g^{-1}, which is far less than the q_{max} derived. Thus, it proves that, at high TC concentration, the adsorbed TC molecules had oriented themselves to accommodate additional layers of TC molecules via hydrophobic interaction.[7]

The maximum adsorption capacity obtained from the Langmuir isotherm model is 257.07 mg g^{-1}. In light of the previous analysis, Fe_3O_4 NPs are responsible for TC removal, which is consistent with the study done by Zhang et al.[10] The maximum adsorption capacity of TC is 500 mg/(g Fe_3O_4 NPs) in their study, and 257.07 mg/(g Fe_3O_4/PAN composite NFs) in ours. As shown in Figure S4 (Supporting Information), which shows thermogravimetric analysis (TGA), the content of the Fe_3O_4 NP coating can be derived from the mass of residual reddish brown Fe_2O_3 (21.21 wt %), and is estimated to be 20.65 wt % (Fe_3O_4). Thus, the maximum adsorption capacity can be converted to 1245 mg/(g Fe_3O_4 NPs). The composite NFs prepared in this study show substantial advantages over the NPs as immobilization prevents NPs from aggregation in the aqueous medium which could reduce the surface area.

A comparison is made between Fe_3O_4/PAN composite NFs and other previously reported adsorbents in Table 2. As shown, 1D NFs were capable of achieving higher or comparable adsorption capacity, demonstrating that deposition of Fe_3O_4 on the PAN NF backbone did not compromise the performance of sole NPs. In addition, considering that antibiotics are usually present at trace level in environmental water bodies, the adsorbent was also tested for the removal of μg/L-ranged TC and oxytetracycline (OTC), while high removal efficiencies (>95% for both TC and OTC) were achieved (Supporting Information Figure S5). Future work will be focused on using Fe_3O_4/PAN composite NFs as adsorbent for the decontamination of effluents from wastewater treatment plant, which usually consist of multiple antibiotics.

3.2.4. Reusability of Fe_3O_4/PAN Composite NFs. The reusability of the adsorbent is considered to be one of the most important criteria to evaluate the feasibility of large scale application. With the observation that the composite NFs exhibited a fairly low adsorption capacity at high pH, 0.01 M NaOH solution was chosen as desorption agent for the regeneration study.

The adsorption−desorption cycles were repeated five times; the results are shown in Figure S6 (Supporting Information). Compared to the virgin composite NFs, the regenerated NFs show excellent reusability and consistency with only 2.72−3.61% decrease in the adsorption efficiency in five cycles. The highly porous and interconnecting pore channeling structure of electronspun NFs reduces the possibility of pore blockage by TC molecules, and enables a close contact between NaOH solution and TC adsorbed; thus, a good regeneration can be achieved.[34] Besides the high surface area, porosity, and adsorption capacity, the excellent reusability of Fe_3O_4/PAN composite NFs demonstrates its great possibility in long-term large scale water treatment, such as advanced wastewater treatment, and household drinking water purification systems. However, further work should be conducted to analyze the cost−benefit.

3.3. Adsorption Mechanism Analysis by XPS. XPS analysis of Fe_3O_4/PAN composite NFs before and after the adsorption of TC was carried out in addition to further investigate the interactions between TC and the composite NFs. Figure 9a gives the wide survey scan of XPS spectra in the range 200−800 eV. No extra peak other than those corresponding to C, N, Fe, and O were observed in the spectra of virgin and adsorbed Fe_3O_4/PAN composite NFs, indicating no impurities formed.

High resolution XPS spectra of Fe 2p of the samples display a typical core level spectrum of Fe_3O_4 consisting two broad peaks positioned at 710.7 and 724.5 eV, which are close to that of Fe_3O_4 NPs reported (Figure 9b).[35] Furthermore, the absence of a satellite peak at 718 eV corresponding to Fe^{3+} ions in γ-Fe_2O_3 concludes that the synthesized composite NFs do not consist of impurities such as γ-Fe_2O_3.[17] The results further confirm that NPs deposited on the surface of PAN NFs were pure Fe_3O_4. After the adsorption of TC on Fe_3O_4 composite NFs, the peak of Fe $2p_{1/2}$ shifted from 724.5 eV (virgin adsorbent) to 724.7 eV, and the peak of Fe $2p_{3/2}$ slightly shifted up by 0.4 to 711.1 eV. The increase of the binding energy of iron indicated the decrease of their electron density, resulting from the forming of Fe−O bonds through a likely complexation between Fe atoms and TC in the adsorption process. The O 1s XPS spectrum of virgin Fe_3O_4/PAN composite NFs can be deconvoluted into three individual component peaks located at 529.6, 531.1, and 532.3 eV (Figure 9c), which are attributed to lattice oxygen in the metal oxide (Fe−O), oxygen atoms in the surface hydroxyl group (H−O), and single carbon−oxygen (C−O) bonds, respectively.[17,36,37] The relative contents of oxygen containing groups in the composite NFs were also calculated and summarized in Table 3. The high peak intensity of the H−O group confirms the abundant presence of hydroxyl groups on the surface of Fe_3O_4/PAN composite NFs. After TC adsorption, the relative content of H−O decreased significantly, suggesting an exchange between surface hydroxyl groups and TC molecules.[38] Meanwhile, the proportion of the Fe−O bond increase implied that the adsorption mechanism was mainly ascribed to the substitution of Fe−OH groups by oxygen containing functional groups of TC, such as C1−C3 tricarbonyl methane moiety and the C10−C12 phenolic diketone moiety.[35] On the basis of the above investigation and pH impact analysis discussed earlier, it is proposed that the adsorption of TC on Fe_3O_4/PAN composite NFs was mainly through the cation exchange and complex formation between the Fe atom from the composite NFs and the deprotonated moieties from the TC molecule (Figure 10).

4. CONCLUSIONS

We report the synthesis of composite NFs with Fe_3O_4 NPs coating via a two-step method, with electrospinning and a subsequent solvothermal process. The as-synthesized Fe_3O_4/PAN composite NFs had a rough surface and an average diameter of 458 ± 38.2 nm. The Fe_3O_4 coating significantly improved the specific surface area of the PAN NFs. Batch adsorption experiments revealed that the composite NFs were effective in removing TC and that there is no impactful loss of Fe to the environment at the pH regime of environmental interest (5−8), with a maximum adsorption capacity (Langmuir isotherm) of 257.07 mg g^{-1} at equilibrium pH of 6, which is comparatively high among the reported adsorbents (Table 2). Good regeneration of Fe_3O_4/PAN composite NFs over numbers of cycles by alkaline rinse further demonstrates that the adsorbent is suitable for long-term scaled up operations.

DOI: 10.1021/acsami.5b04598
ACS Appl. Mater. Interfaces 2015, 7, 14573−14583

The underlying mechanism of TC adsorption was investigated by pH impact study and XPS analysis. The dominant interaction was the surface complexation between TC and the composite NFs. The present work suggests that Fe_3O_4/PAN composite NFs, owing to their simple preparation procedures, high adsorption capacity, good regenerability, low cost, and environmentally benign nature, have great potential as the next-generation adsorbent in the removal of antibiotics and other emerging contaminants.

■ ASSOCIATED CONTENT

Supporting Information

Chemical structure and acid dissociation constants of TC (Scheme S1), operating parameters in the experiments for the optimization of ratio of $FeCl_3$ to PAN NFs (Table S1), morphology of Fe_3O_4/PAN composite NFs (Figure S1), TC adsorption capacities on Fe_3O_4/PAN composite NF with varying $FeCl_3$ to PAN NFs dosage ratios (Figure S2), comparison between TC adsorption on PAN NFs and Fe_3O_4/PAN composite NFs (Figure S3), thermogravimetric analysis (TGA) curve of Fe_3O_4/PAN composite NFs (Figure S4), adsorption of TC and OTC on Fe_3O_4/PAN composite NFs (Figure S5), and reusability of the Fe_3O_4/PAN composite NFs for TC removal (Figure S6). The Supporting Information is available free of charge on the ACS Publications website at DOI: 10.1021/acsami.5b04598.

■ AUTHOR INFORMATION

Corresponding Author

*Phone:+86-592-6190785. E-mail: ymzheng@iue.ac.cn.

Notes

The authors declare no competing financial interest.

■ ACKNOWLEDGMENTS

This work was partially funded by the Hundred Talents Program of Chinese Academy of Sciences, the Key Project of Science and Technology Program of Fujian Province (2013H0054), and the Science and Technology Innovation and Collaboration Team Project of the Chinese Academy of Sciences.

■ REFERENCES

(1) Sarmah, A. K.; Meyer, M. T.; Boxall, A. B. A Global Perspective on the Use, Sales, Exposure Pathways, Occurrence, Fate and Effects of Veterinary Antibiotics (VAs) in the Environment. *Chemosphere* **2006**, *65*, 725−759.

(2) Zhu, Y. G.; Johnson, T. A.; Su, J. Q.; Qiao, M.; Guo, G. X.; Stedtfeld, R. D.; Hashsham, S. A.; Tiedje, J. M. Diverse and Abundant Antibiotic Resistance Genes in Chinese Swine Farms. *Proc. Natl. Acad. Sci. U.S.A.* **2013**, *110*, 3435−3440.

(3) Hao, R.; Xiao, X.; Zuo, X.; Nan, J.; Zhang, W. Efficient Adsorption and Visible-Light Photocatalytic Degradation of Tetracycline Hydrochloride Using Mesoporous BiOI Microspheres. *J. Hazard. Mater.* **2012**, *209−210*, 137−145.

(4) Le-Minh, N.; Khan, S. J.; Drewes, J. E.; Stuetz, R. M. Fate of Antibiotics During Municipal Water Recycling Treatment Processes. *Water Res.* **2010**, *44*, 4295−4323.

(5) Figueroa, R. A.; Leonard, A.; Mackay, A. A. Modeling Tetracycline Antibiotic Sorption to Clays. *Environ. Sci. Technol.* **2004**, *38*, 476−483.

(6) Figueroa, R. A.; Mackay, A. A. Sorption of Oxytetracycline to Iron Oxides and Iron Oxide-Rich Soils. *Environ. Sci. Technol.* **2005**, *39*, 6664−6671.

(7) Gu, C.; Karthikeyan, K. G. Interaction of Tetracycline with Aluminum and Iron Hydrous Oxide. *Environ. Sci. Technol.* **2005**, *39*, 2660−2667.

(8) Schmitt, M. O.; Schneider, S. Spectroscopic Investigation of Complexation between Various Tetracyclines and Mg^{2+} or Ca^{2+}. *PhysChemComm* **2000**, *9*, 42−55.

(9) Ma, Y.; Zhou, Q.; Li, A.; Shuang, C.; Shi, Q.; Zhang, M. Preparation of a Novel Magnetic Microporous Adsorbent and Its Adsorption Behavior of p-Nitrophenol and Chlorotetracycline. *J. Hazard. Mater.* **2014**, *266*, 84−93.

(10) Zhang, D.; Niu, H.; Zhang, X.; Meng, Z.; Cai, Y. Strong Adsorption of Chlorotetracycline on Magnetite Nanoparticles. *J. Hazard. Mater.* **2011**, *192*, 1088−1093.

(11) Ambashta, R. D.; Sillanpaa, M. Water Purification Using Magnetic Assistance: A Review. *J. Hazard. Mater.* **2010**, *180*, 38−49.

(12) Zhang, Z.; Shao, C.; Li, X.; Wang, C.; Zhang, M.; Liu, Y. Electrospun Nanofibers of p-Type NiO/n-Type ZnO Heterojunctions with Enhanced Photocatalytic Activity. *ACS Appl. Mater. Interfaces* **2010**, *2*, 2915−2923.

(13) Regonini, D.; Teloeken, A. C.; Alves, A. K.; Berutti, F. A.; Gajda-Schrantz, K.; Bergmann, C. P.; Graule, T.; Clemens, F. Electrospun TiO_2 Fiber Composite Photoelectrodes for Water Splitting. *ACS Appl. Mater. Interfaces* **2013**, *5*, 11747−11755.

(14) Raza, A.; Ding, B.; Zainab, G.; El-Newehy, M.; Al-Deyab, S. S.; Yu, J. In Situ Cross-Linked Superwetting Nanofibrous Membranes for Ultrafast Oil-Water Separation. *J. Mater. Chem. A* **2014**, *2*, 10137−10145.

(15) Peng, X.; Santulli, A. C.; Sutter, E.; Wong, S. S. Fabrication and Enhanced Photocatalytic Activity of Inorganic Core−Shell Nanofibers Produced by Coaxial Electrospinning. *Chem. Sci.* **2012**, *3*, 1262−1272.

(16) Fratoddi, I.; Macagnano, A.; Battocchio, C.; Zampetti, E.; Venditti, I.; Russo, M. V.; Bearzotti, A. Platinum Nanoparticles on Electrospun Titania Nanofibers as Hydrogen Sensing Materials Working at Room Temperature. *Nanoscale* **2014**, *6*, 9177−9184.

(17) Mu, J.; Chen, B.; Guo, Z.; Zhang, M.; Zhang, Z.; Zhang, P.; Shao, C.; Liu, Y. Highly Dispersed Fe_3O_4 Nanosheets on One-Dimensional Carbon Nanofibers: Synthesis, Formation Mechanism, and Electrochemical Performance as Supercapacitor Electrode Materials. *Nanoscale* **2011**, *3*, 5034−5040.

(18) Chen, M.; Wang, C.; Fang, W.; Wang, J.; Zhang, W.; Jin, G.; Diao, G. Electrospinning of Calixarene-Functionalized Polyacrylonitrile Nanofiber Membranes and Application as an Adsorbent and Catalyst Support. *Langmuir* **2013**, *29*, 11858−11867.

(19) Teng, M.; Qiao, J.; Li, F.; Bera, P. K. Electrospun Mesoporous Carbon Nanofibers Produced from Phenolic Resin and Their Use in the Adsorption of Large Dye Molecules. *Carbon* **2012**, *50*, 2877−2886.

(20) Zhang, D.; Karki, A. B.; Rutman, D.; Young, D. P.; Wang, A.; Cocke, D.; Ho, T. H.; Guo, Z. Electrospun Polyacrylonitrile Nanocomposite Fibers Reinforced with Fe_3O_4 Nanoparticles: Fabrication and Property Analysis. *Polymer* **2009**, *50*, 4189−4198.

(21) Ji, L.; Wan, Y.; Zheng, S.; Zhu, D. Adsorption of Tetracycline and Sulfamethoxazole on Crop Residue-Derived Ashes: Implication for the Relative Importance of Black Carbon to Soil Sorption. *Environ. Sci. Technol.* **2011**, *45*, 5580−5586.

(22) Shen, L.-H.; Bao, J.-F.; Wang, D.; Wang, Y.-X.; Chen, Z.-W.; Ren, L.; Zhou, X.; Ke, X.-B.; Chen, M.; Yang, A.-Q. One-Step Synthesis of Monodisperse, Water-Soluble Ultra-Small Fe_3O_4 Nanoparticles for Potential Bio-Application. *Nanoscale* **2013**, *5*, 2133−2141.

(23) Bourikas, K.; Vakros, J.; Kordulis, C.; Lycourghiotis, A. Potentiometric Mass Titrations Experimental and Theoretical Establishment of a New Technique for Determining the Point of Zero Charge (PZC) of Metal (Hydr)Oxides. *J. Phys. Chem. B* **2003**, *107*, 9441−9451.

(24) Hou, H.; Ge, J. J.; Zeng, J.; Li, Q.; Reneker, D. H.; Greiner, A.; Cheng, S. Z. D. Electrospun Polyacrylonitrile Nanofibers Containing a High Concentration of Well-Aligned Multiwall Carbon Nanotubes. *Chem. Mater.* **2005**, *17*, 967−973.

(25) Xiao, L.; Li, J.; Brougham, D. F.; Fox, E. K.; Feliu, N.; Bushmelev, A.; Schmidt, A.; Mertens, N.; Kiessling, F.; Valldor, M.

DOI: 10.1021/acsami.5b04598
ACS Appl. Mater. Interfaces 2015, 7, 14573−14583

Water-Soluble Superparamagnetic Magnetite Nanoparticles with Biocompatible Coating for Enhanced Magnetic Resonance Imaging. *ACS Nano* **2011**, *5*, 6315−6324.
(26) Zhang, S.; Xu, W.; Zeng, M.; Li, J.; Li, J.; Xu, J.; Wang, X. Superior Adsorption Capacity of Hierarchical Iron Oxide@Magnesium Silicate Magnetic Nanorods for Fast Removal of Organic Pollutants from Aqueous Solution. *J. Mater. Chem. A* **2013**, *1*, 11691−11697.
(27) Zheng, Y. M.; Lim, S. F.; Chen, J. P. Preparation and Characterization of Zirconium-Based Magnetic Sorbent for Arsenate Removal. *J. Colloid Interface Sci.* **2009**, *338*, 22−29.
(28) Duan, L.; Li, L.; Xu, Z.; Chen, W. Adsorption of Tetracycline to Nano-NiO: the Effect of Co-Existing Cu(II) Ions and Environmental Implications. *Environ. Sci.: Processes Impacts* **2014**, *16*, 1462−1468.
(29) Ling, C.; Liu, F. Q.; Xu, C.; Chen, T. P.; Li, A. M. An Integrative Technique Based on Synergistic Coremoval and Sequential Recovery of Copper and Tetracycline with Dual-Functional Chelating Resin: Roles of Amine and Carboxyl Groups. *ACS Appl. Mater. Interfaces* **2013**, *5*, 11808−11817.
(30) Gao, Y.; Li, Y.; Zhang, L.; Huang, H.; Hu, J.; Shah, S. M.; Su, X. Adsorption and Removal of Tetracycline Antibiotics from Aqueous Solution by Graphene Oxide. *J. Colloid Interface Sci.* **2012**, *368*, 540−546.
(31) Zhao, Y.; Geng, J.; Wang, X.; Gu, X.; Gao, S. Adsorption of Tetracycline onto Goethite in the Presence of Metal Cations and Humic Substances. *J. Colloid Interface Sci.* **2011**, *361*, 247−251.
(32) Zhang, S.; Zeng, M.; Li, J.; Li, J.; Xu, J.; Wang, X. Porous Magnetic Carbon Sheets from Biomass as an Adsorbent for the Fast Removal of Organic Pollutants from Aqueous Solution. *J. Mater. Chem. A* **2014**, *2*, 4391−4397.
(33) Zhao, G.; Jiang, L.; He, Y.; Li, J.; Dong, H.; Wang, X.; Hu, W. Sulfonated Graphene for Persistent Aromatic Pollutant Management. *Adv. Mater.* **2011**, *23*, 3959−3963.
(34) Kim, E. J.; Lee, C. S.; Chang, Y. Y.; Chang, Y. S. Hierarchically Structured Manganese Oxide-Coated Magnetic Nanocomposites for the Efficient Removal of Heavy Metal Ions from Aqueous Systems. *ACS Appl. Mater. Interfaces* **2013**, *5*, 9628−9234.
(35) Wang, T.; Zhang, L.; Wang, H.; Yang, W.; Fu, Y.; Zhou, W.; Yu, W.; Xiang, K.; Su, Z.; Dai, S.; Chai, L. Controllable Synthesis of Hierarchical Porous Fe_3O_4 Particles Mediated by Poly(diallyldimethylammonium chloride) and Their Application in Arsenic Removal. *ACS Appl. Mater. Interfaces* **2013**, *5*, 12449−12459.
(36) Lim, S.-F.; Zheng, Y.-M.; Zou, S.-W.; Chen, J. P. Characterization of Copper Adsorption onto an Alginate Encapsulated Magnetic Sorbent by a Combined FT-IR, XPS, and Mathematical Modeling Study. *Environ. Sci. Technol.* **2008**, *42*, 2551−2556.
(37) Górska, P.; Zaleska, A.; Kowalska, E.; Klimczuk, T.; Sobczak, J. W.; Skwarek, E.; Janusz, W.; Hupka, J. TiO_2 Photoactivity in vis and UV Light: The Influence of Calcination Temperature and Surface Properties. *Appl. Catal., B* **2008**, *84*, 440−447.
(38) Cao, C.-Y.; Qu, J.; Yan, W.-S.; Zhu, J.-F.; Wu, Z.-Y.; Song, W.-G. Low-Cost Synthesis of Flowerlike α-Fe_2O_3 Nanostructures for Heavy Metal Ion Removal: Adsorption Property and Mechanism. *Langmuir* **2012**, *28*, 4573−4579.
(39) Shi, Y.-J.; Wang, X.-H.; Qi, Z.; Diao, M.-H.; Gao, M.-M.; Xing, S.-F.; Wang, S.-G.; Zhao, X.-C. Sorption and Biodegradation of Tetracycline by Nitrifying Granules and the Toxicity of Tetracycline on Granules. *J. Hazard. Mater.* **2011**, *191*, 103−109.
(40) Liao, P.; Zhan, Z.; Dai, J.; Wu, X.; Zhang, W.; Wang, K.; Yuan, S. Adsorption of Tetracycline and Chloramphenicol in Aqueous Solutions by Bamboo Charcoal: A batch and Fixed-Bed Column Study. *Chem. Eng. J.* **2013**, *228*, 496−505.
(41) Kang, J.; Liu, H.; Zheng, Y.-M.; Qu, J.; Chen, J. P. Systematic Study of Synergistic and Antagonistic Effects on Adsorption of Tetracycline and Copper onto a Chitosan. *J. Colloid Interface Sci.* **2010**, *344*, 117−125.
(42) Zhang, Y.; Chen, B.; Zhang, L.; Huang, J.; Chen, F.; Yang, Z.; Yao, J.; Zhang, Z. Controlled Assembly of Fe_3O_4 Magnetic Nanoparticles on Graphene Oxide. *Nanoscale* **2011**, *3*, 1446−1450.

DOI: 10.1021/acsami.5b04598
ACS Appl. Mater. Interfaces 2015, 7, 14573−14583